CORA Cork Open Research Archive
Cartlann Taighde Oscailte Chorcaí

Title	Low-power actuators for programmable photonic processors
Authors	Khan, Muhammad Umar;Zand, Iman;Van Iseghem, Lukas;Edinger, Pierre;Jo, Gaehun;Bleiker, Simon J.;Takabayashi, Alain Y.;Antony, Cleitus;Jezzini, Moises;Talli, Giuseppe;Sattari, Hamed;Lee, Jun Su;Mallik, Arun Kumar;Verheyen, Peter;Lerma Arce, Cristina;Garcia Porcel, Marco;Jonuzi, Tigers;Picavet, Ewout;Nagarjun, K. P.;Watté, Jan;Quack, Niels;Niklaus, Frank;Gylfason, K. B.;De Buysser, Klaartje;Beeckman, Jeroen;Bogaerts, Wim
Publication date	2023-03-15
Original Citation	Khan, U., Zand, I., Van Iseghem, L., Edinger, P., Jo, G., Bleiker, S. J., Takabayashi, A. Y., Antony, C., Jezzini, M., Talli, G., Sattari, H., Lee, J. S., Mallik, A. K., Verheyen, P., Lerma Arce, C., Garcia, M., Jonuzi, T., Picavet, E., Nagarjun, K. P., Watté, J., Quack, N., Niklaus, F., Gylfason, K. B., De Buysser, K., Beeckman, J. and Bogaerts, W. (2023) 'Low-power actuators for programmable photonic processors', Proceedings of SPIE, 12438, AI and Optical Data Sciences IV, 124380K, pp. 142-153. https://doi.org/10.1117/12.2647371
Type of publication	Article (peer-reviewed);Conference item
Link to publisher's version	10.1117/12.2647371
Rights	© 2023, Society of Photo-Optical Instrumentation Engineers (SPIE). One print or electronic copy may be made for personal use only. Systematic reproduction and distribution, duplication of any material in this publication for a fee or for commercial purposes, and modification of the contents of the publication are prohibited.
Download date	2026-10-24 21:03:04
Item downloaded from	https://hdl.handle.net/10468/17178



University College Cork, Ireland
Coláiste na hOllscoile Corcaigh

PROCEEDINGS OF SPIE

SPIEDigitalLibrary.org/conference-proceedings-of-spie

Low-power actuators for programmable photonic processors

Umar Khan, Iman Zand, Lukas Van Iseghem, Pierre Edinger, Gaehun Jo, et al.

Umar Khan, Iman Zand, Lukas Van Iseghem, Pierre Edinger, Gaehun Jo, Simon J. Bleiker, Alain Yuji Takabayashi, Cleitus Antony, Moises Jezzini, Giuseppe Talli, Hamed Sattari, Jun Su Lee, Arun Kumar Mallik, Peter Verheyen, Cristina Lerma Arce, Marco Garcia, Tigers Jonuzi, Ewout Picavet, K. P. Nagarjun, Jan Watté, Niels Quack, Frank Niklaus, Kristinn B. Gylfason, Klaartje De Buysser, Jeroen Beeckman, Wim Bogaerts, "Low-power actuators for programmable photonic processors," Proc. SPIE 12438, AI and Optical Data Sciences IV, 124380K (15 March 2023); doi: 10.1117/12.2647371

SPIE.

Event: SPIE OPTO, 2023, San Francisco, California, United States

Downloaded From: https://www.spiedigitallibrary.org/conference-proceedings-of-spie on 24 Mar 2023 Terms of Use: https://www.spiedigitallibrary.org/terms-of-use

Invited Paper

Low power actuators for programmable photonic processors

Umar Khan[a,b], Iman Zand[a,b], Lukas Van Iseghem[a, b], Pierre Edinger[d], Gaehun Jo[d], Simon J. Bleiker[d], Alain Yuji Takabayashi[c], Cleitus Antony[f], Moises Jezzini[f], Giuseppe Talli[f], Hamed Sattari[c], Jun Su Lee[f], Arun Kumar Mallik[f], Peter Verheyen[e], Cristina Lerma Arce[g], Marco Garcia[h], Tigers Jonuzi[h], Ewout Picavet[i,j], K. P. Nagarjun[a,b], Jan Watte[g], Niels Quack[c], Frank Niklaus[d], Kristinn B. Gylfason[d], Klaartje De Buysser[i,j], Jeroen Beeckman[i,j], and Wim Bogaerts[a,b]

[a]Ghent University - IMEC, Department of Information Technology, Photonics Research Group, Technologiepark-Zwijnaarde, Ghent, Belgium
[b]Center of Nano- and Biophotonics, Ghent University, Ghent, Belgium
[c]École Polytechnique Fédérale de Lausanne (EPFL), 1015 Lausanne, Switzerland.
[d]KTH Royal Institute of Technology, SE-100 44 Stockholm, Sweden.
[e]imec vzw. 3DSIP Department, Si Photonics Group, Kapeldreef 75, 3001 Leuven, Belgium
[f]Tyndall National Institute, Lee Maltings Complex Dyke Parade, T12 R5CP Cork, Ireland
[g]Commscope Connectivity Belgium, Diestsesteenweg 692, 3010 Kessel LO, Belgium
[h] VLC Photonics S.L., Ed. 9B, D2, UPV, Camino de vera sn, 46022 Valencia, Spain
[i]Sol-gel Centre for Research on Inorganic Powders and Thin films Synthesis, Ghent University, Dept. of Chemistry, Belgium
[j]Liquid Crystals and Photonics Group, Ghent University, Dept. of Electronics and Information Systems, Belgium

ABSTRACT

The demand for efficient actuators in photonics has peaked with increasing popularity for large-scale general-purpose programmable photonics circuits. We present our work to enhance an established silicon photonics platform with low-power *micro-electromechanical* (MEMS) and *liquid crystal* (LC) actuators to enable large-scale programmable *photonic integrated circuits* (PICs).

Keywords: Silicon Photonics, Programmable Photonics, Micro-Electromechanical Systems (MEMS), Liquid Crystals (LC), low-power actuators, Photonic integrated circuits (PIC)

1. INTRODUCTION

Recent broadening of the application base for photonics has resulted in the emergence of different material platforms.[1–8] Out of these platforms, silicon photonics taking advantage of high integration density and its compatibility with traditional semiconductor manufacturing techniques has emerged as one of the most prominent and industrially scalable technology for *photonic integrated circuits* (PIC). It is still challenging to make large-scale photonic circuits for even the most mature platform due to the fabrication variability over the wafer.[9–11] A

Further author information: (Send correspondence to U.K)
U.K.: E-mail: umar.khan@ugent.be
W.B.: E-mail: wim.bogaerts@ugent.be
K.B.G: E-mail: gylfason@kth.se
N.Q was previously at EPFL and is now at The University of Sydney, Australia. E-mail: niels.quack@sydney.edu.au
A.Y. T and H.S. are no longer at EPFL.
M.J., G.T. and M.S. are no longer at Tyndall National Institute.
M.G is no longer at VLC Photonics.

AI and Optical Data Sciences IV, edited by Bahram Jalali, Ken-ichi Kitayama,
Proc. of SPIE Vol. 12438, 124380K · © 2023 SPIE
0277-786X · doi: 10.1117/12.2647371

Downloaded From: https://www.spiedigitallibrary.org/conference-proceedings-of-spie on 24 Mar 2023
Terms of Use: https://www.spiedigitallibrary.org/terms-of-use

solution to this problem is using active tuners/actuators (here tuners and actuators are used interchangeably). These are devices that can adjust the properties of the waveguides in real time, allowing them to compensate for variations in the fabrication process. Active tuners can be integrated into the photonic circuits and controlled by an external controller. This is especially important in large-scale photonic circuits, where the impact of these variabilities can be significant. Large-scale programmable photonic circuits capable of configuring the light path using the software have recently gained much attention. The use of active tuners is most pronounced in large-scale programmable photonic circuits as hundreds or even thousands of electronically controlled active tuners (phase shifters or tunable couplers) are required to configure the light path on the chip.

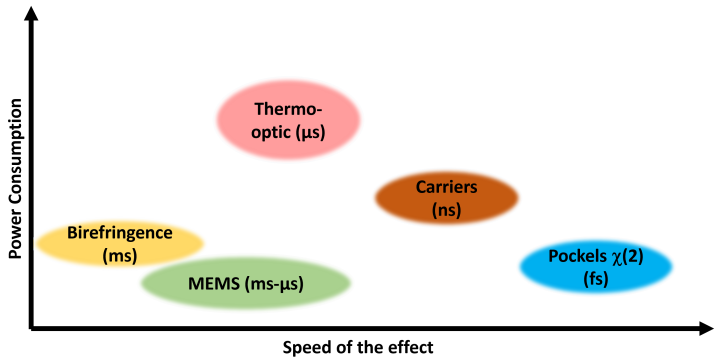


Figure 1. A semi-quantitative comparison (in terms of speed of the effect and the power consumption) among different available actuation mechanisms for silicon photonics.

2. ACTUATORS FOR PROGRAMMABLE PHOTONICS

A large-scale general-purpose programmable photonic circuit can require up to thousands of tuners (phase shifters and tunable couplers) along with other high-performance components such as modulators and detectors.[12–17] Different tuners based on the thermo-optic,[18–20] carrier-based,[21,22] liquid crystal,[23–31] and Pockels effects[32,33] have already been investigated, Figure 1. Among these, thermo-optic tuners using a heater placed in proximity of the optical waveguide for tuning are widely adopted owing to the simple fabrication process for silicon photonics. However, it is a challenge to integrate tuners in large numbers, even for the commonly used thermo-optic tuners, because these tuners are power-hungry, require sufficient spacing to avoid thermal cross-talk and are relatively slow with response time in micro to milliseconds. This highlights the need for an improvement in the efficiency of the thermo-optic tuners. A lot of effort has been put into making thermo-optic tuners more efficient in terms of power consumption and speed.[34–36]

The other phase-shifting mechanism which is natively present in silicon photonics is the carriers-based plasma dispersion effect.[21,22] This mechanism is most suited for fast modulation but suffers from high insertion losses, and large footprints making it not suitable for general-purpose programmable circuits. Due to the lack of second-order non-linearity, electro-optic (EO) phase shifting mechanisms are negligible for silicon and require heterogeneous integration of EO materials (e.g. lithium niobate ($LiNbO_3$), and graphene) which are not that straightforward to integrate with an existing silicon photonic platform.[32,33,37,38]

Thus, a more efficient (low power consumption, low insertion loss, small footprint) tuning mechanism is required that can be integrated directly with other functional building blocks of the silicon photonics platform. In this paper, we present our work to extend an established silicon photonics platform with low-power *micro-electromechanical* (MEMS) and *liquid crystal* (LC) based actuators, Figure 2.

3. MICRO-ELECTROMECHANICAL (MEMS)

Micro-electromechanical systems (MEMS) can be used to manipulate light on a chip utilizing the mechanical movement of the waveguides. With this movement, it is possible to induce a phase shift or to directly change

Downloaded From: https://www.spiedigitallibrary.org/conference-proceedings-of-spie on 24 Mar 2023
Terms of Use: https://www.spiedigitallibrary.org/terms-of-use

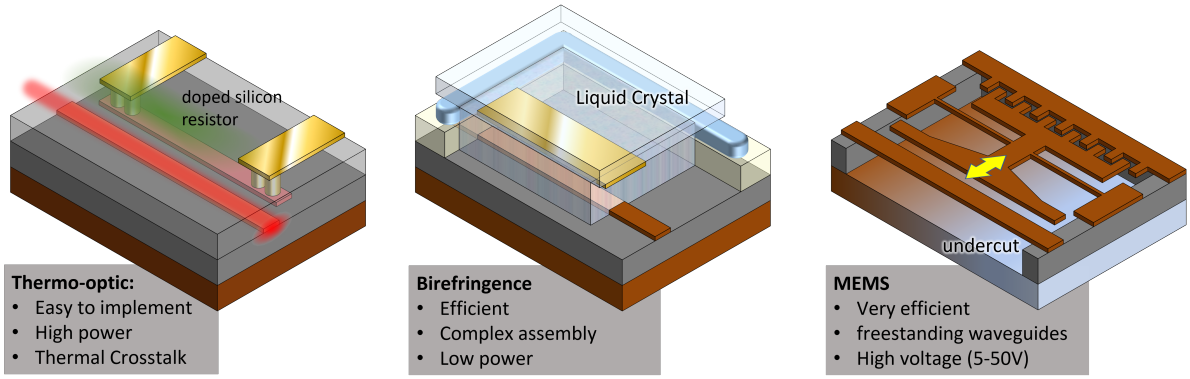


Figure 2. Sketches representing different tuning mechanisms for silicon photonics. Thermo-optic: heat dissipated across a heater (Tungsten or doped-silicon) changes the refractive index of the waveguide and the surrounding material. Birefringence: liquid crystal is used as a cladding material for the waveguide. Change in the orientation of the liquid crystal molecules results in a change in refractive index. MEMS: mechanical movement results in a change of refractive index around the waveguide.

the coupling between two waveguides. MEMS-based phase shifters,[39–43] tunable couplers,[44,45] switches,[46–50] and tunable filters[51,52] have already been demonstrated using different specialized platforms. Programmable photonic circuits require efficient tuners along with other high-performance building blocks like modulators and detectors from an established platform. But, integration of MEMS with a standard silicon photonics platform is not that straightforward because optical waveguides are buried underneath a *back-end-of-line* (BEOL) layer stack containing different metal and dielectric layers. This highlights the need for enhancing of an already established silicon photonic platform with MEMS actuators.

Here, we present our work in enhancing of an established silicon photonic platform from IMEC, iSiPP50G, with MEMS. This platform provides high-performance passives, possibilities of different doping profiles, tungsten and doped-silicon heaters, variations of modulators and photodetectors capable of operating beyond 50Gbps, and two metal layers for the electrical routing.[53] A wafer-level post-processing flow is developed to selectively remove the *back-end-of-line* (BEOL) dielectric stack and the oxide underneath the optical waveguides using different masking and *hydrofluoric acid* (HF) etching steps.[54,55]

Figure 3 summarizes the developed process flow for the enhancement of the iSiPP50G silicon photonics platform with MEMS. It can be noticed from the cross-section that the *back-end-of-line* (BEOL) layer stack consists of different metal and dielectric layers. When enhancing an established silicon photonics platform with MEMS by selectively etching the oxide underneath the waveguides, these layers must be adequately protected to avoid etching in the lateral direction. The top most cross-section shown in step 1 of Figure 3 represents the sample after the BEOL opening on top of the MEMS regions. The BEOL opening module is the standard module of iSiPP50G and is usually used for applications such as sensing which requires exposure of the waveguides from the top. While developing the MEMS release process flow, a major feature included appropriate protection of the BEOL stack from *vapour phase hydrofluoric acid* (vHF), which will not only attack the oxide around the waveguides but also the side walls of the recess/cavity (formed after removal of the BEOL) resulting in collapse of the BEOL layers. *Atomic layer deposition* (ALD) deposited *aluminium oxide* (AlOx) was used to protect the BEOL from the unwanted etching. As ALD is a very conformal deposition method, all side-walls and the corners within the cavity are well covered with AlOx and prevents etching of the BEOL stack. Before the deposition of the AlOx protective layer, the oxide next to the waveguides was removed using a *buffered hydrofluoric acid* (bHF) etch. The side-oxide was removed to make sure that AlOx gets deposited on the silicon to prevent vHF access to the BEOL layers. The cross-section in step 2 of Figure 3 represents the sample after the removal of the side-oxide. AlOx is deposited using ALD and then local windows are opened on top of the bond-pads and the MEMS devices for removal of the buried oxide using vHF. The cross-section in step 3 of Figure 3 represents the sample after the deposition and opening of the protective AlOx layer. Now that the sample is well-protected against the vHF everywhere except the MEMS cavity regions, vHF is used to remove the oxide underneath the

Downloaded From: https://www.spiedigitallibrary.org/conference-proceedings-of-spie on 24 Mar 2023
Terms of Use: https://www.spiedigitallibrary.org/terms-of-use

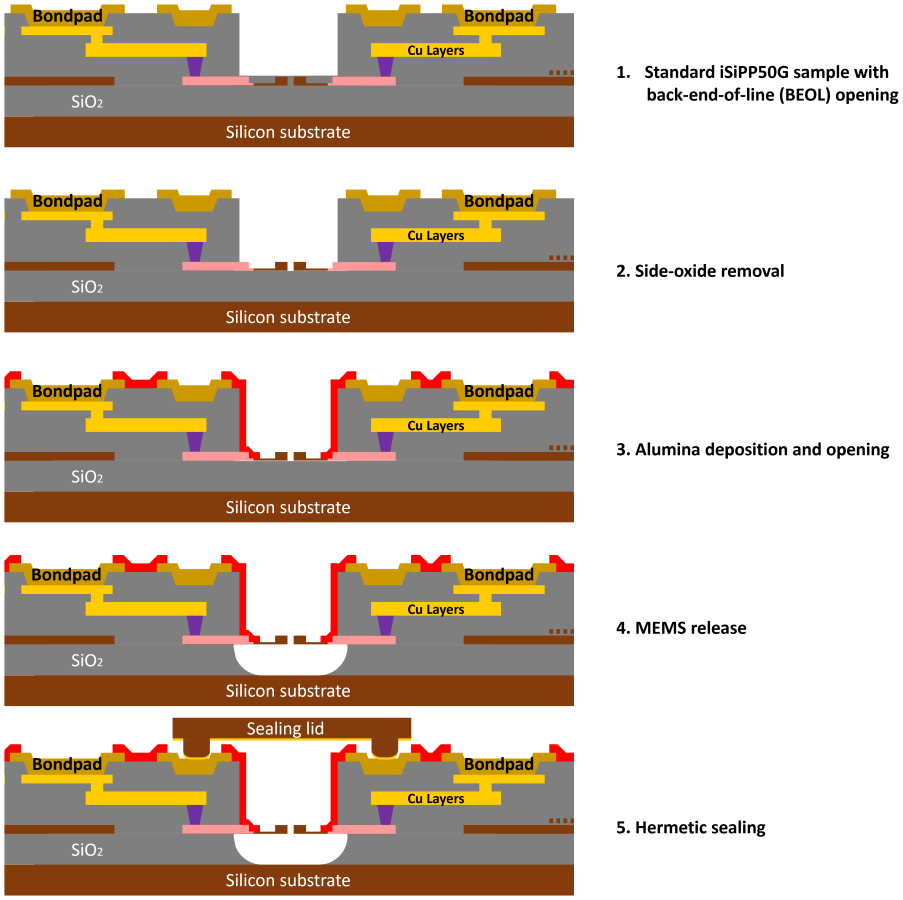


Figure 3. Sketches showing the cross-sections of the sample after major steps of the process flow. Step 1 represents the state after the removal of *back-end-of-line* (BEOL) stack using the standard iSiPP50G module. Step 2 represents the state after the removal of the side oxide cladding using *buffered hydrofluoric acid* (bHF). Step 3 represents the state after the deposition and opening of a thin *aluminium oxide* (AlOx) protective layer. Step 4 represents the released MEMS after the etching using *vapour phase hydrofluoric* (vHF) acid. Step 5 represents the hermetically sealed sample.

waveguides. As this is an isotropic etch process, the oxide is attacked both in the downwards and the lateral directions. At least $2\mu m$ of oxide is removed by the vHF etch to fully clear the silicon substrate underneath the freestanding waveguides. A solid ring of silicon is used as a buffer to protect the leaking of the vHF to the BEOL through the buried oxide region. The cross-section in step 4 of Figure 3 shows the released MEMS after the removal of the buried oxide. To protect the suspended regions of the MEMS structures from environmental influences (dust, humidity etc.), the MEMS device cavities were hermetically sealed after the etching of the buried oxide. The cross-section in step 5 of Figure 3 represents the sample after hermetic sealing of the released MEMS cavities. Wafer-level hermetic sealing of MEMS cavities is discussed in section 3.3.

3.1 Phase Shifter

A compact low-power phase shifter for large-scale programmable photonic circuits is experimentally demonstrated using the above-explained process flow.[41] The designed phase shifter consists of an air-clad optical waveguide and a narrow silicon beam positioned in close proximity of the waveguide. The narrow silicon beam is in optical cut-off at the operating wavelength of 1550 nm and acts only as an index perturbation when brought very close to the waveguide. The distance between the optical waveguide and the narrow silicon beam is varied using electrostatic forces to induce a phase shift. It can be noticed in Figure 4 (a) that the narrow silicon beam is connected to an H-shaped shuttle. With the application of a voltage across the comb drive (i.e. between the

Downloaded From: https://www.spiedigitallibrary.org/conference-proceedings-of-spie on 24 Mar 2023
Terms of Use: https://www.spiedigitallibrary.org/terms-of-use

H-shaped shuttle and the fixed electrode), an electrostatic attractive force is generated that pulls the shuttle and narrow silicon beam away from the waveguide. The springs shown in the inset of Figure 4 (a) provide a restoring force and the shuttle moves back to its equilibrium state as the voltage is removed. Phase shifters with different restoring springs' lengths were designed to evaluate the trade-off between operation voltage and device speed. The length of the restoring springs affects the device stiffness, which results in different voltages required for a π phase shift. To characterize the phase shift induced by the MEMS phase shifter, an unbalanced *Mach-Zehnder interferometer* (MZI) was designed to have a MEMS phase shifter in one of the paths. It can be noticed in Figure 4 (b) that the required voltage for π phase shift decreases with increasing length of the spring. Longer springs are softer (less stiff) requiring a smaller voltage (electrostatic force) to achieve the same amount of displacement. This decrease in the stiffness of the spring can also be noticed from the frequency responses plotted in Figure 4 (c). The resonance frequency lowers with reduced stiffness and thus, is imposing a restriction on the maximum actuation speed of the phase shifter.

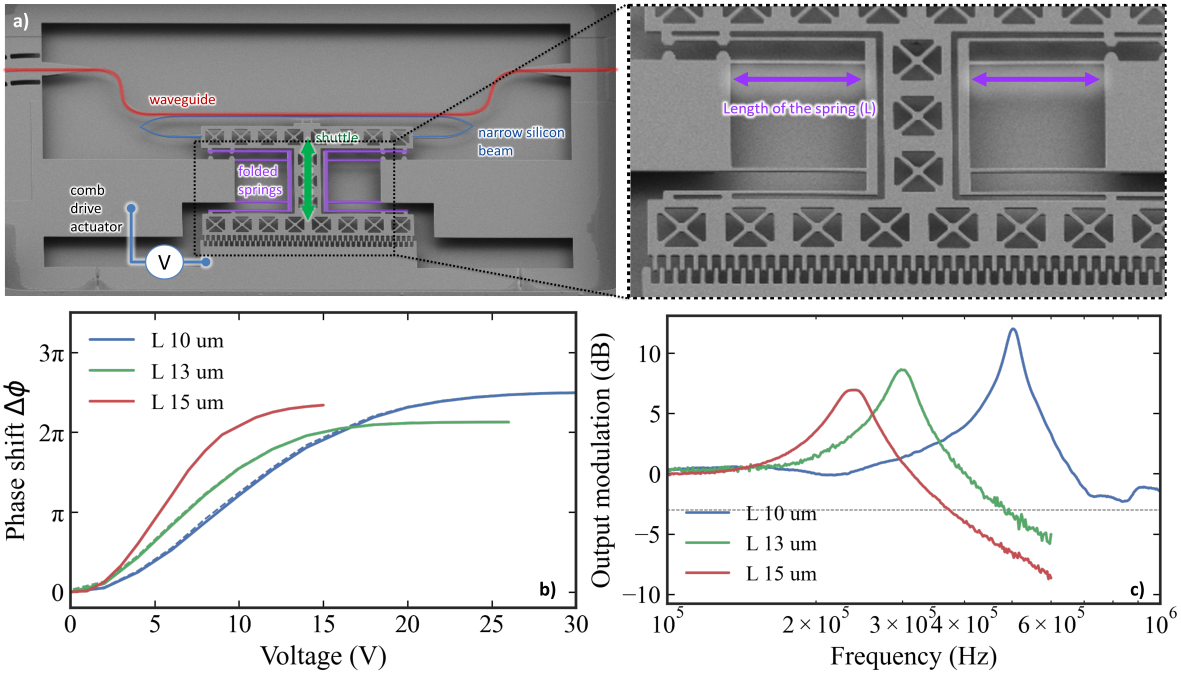


Figure 4. (a) Scanning electron microscope (SEM) image of the MEMS-based phase shifter. The optical waveguide, narrow silicon beam, comb drive and the shuttle that moves with the application of the bias voltage are annotated. The inset shows the length of the restoring spring (L) that is varied to achieve different values of voltages required for π phase shift. (b) Graphs showing the measured phase shift for different bias voltages. It can be noticed from the graphs that the voltage required for achieving π phase shift decreases with increasing spring length. (c) Graphs showing the resonance frequency of different sprint lengths (L). The resonance frequency decreases with increasing spring length.

3.2 Tunable Coupler

Passive optical components like *directional couplers* (DC)[56–59] or *multi mode interferometers* (MMI)[60–63] having fixed splitting ratios are usually used for the splitting of light within an optical circuit. For programmable photonic circuits, *Mach-Zehnder interferometers* (MZI) using thermo-optic phase shifters are usually used to attain tunable coupling.[64–66] This tunability comes at a cost of a larger footprint and power consumption of several milliwatts. In order to overcome these power consumption and real estate issues, a compact and low-power MEMS-based broadband 2×2 tunable coupler[45] was experimentally demonstrated for the MEMS-enhanced silicon photonics platform. A *scanning electron microscope* (SEM) image of the fabricated tunable coupler is shown in Figure 5 (a). Notice that one arm of the evanescent coupler is fixed while another arm is

Downloaded From: https://www.spiedigitallibrary.org/conference-proceedings-of-spie on 24 Mar 2023
Terms of Use: https://www.spiedigitallibrary.org/terms-of-use

connected to the comb drive facilitating the mechanical movement. The application of a voltage across the comb drive generates an electrostatic force resulting in a variation of the gap between the suspended waveguides and ultimately resulting in different coupling ratios. Figure 5 (b) shows that a broadband (> 35 nm) optical power coupling with an extinction ratio of 25 dB was achieved for the designed wavelength of $\lambda = 1550$ nm.

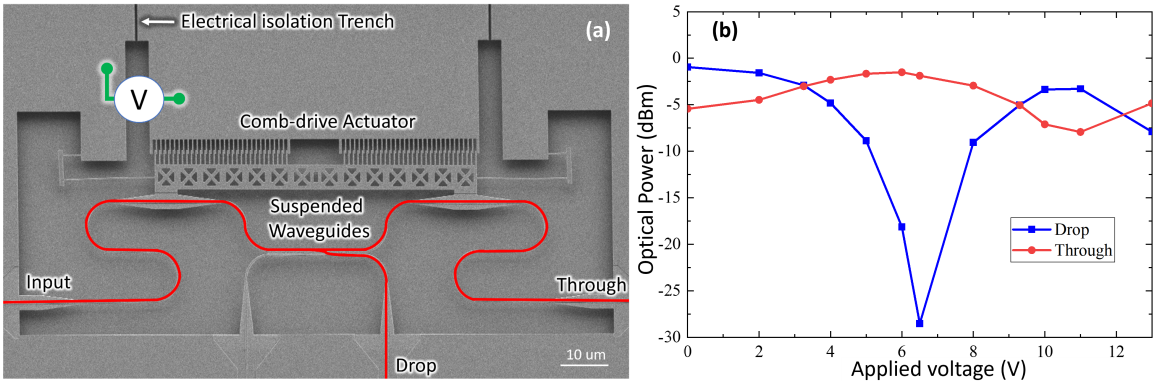


Figure 5. (a) Scanning electron microscope (SEM) image of the MEMS-based tunable coupler. Optical ports, light paths within the coupler, comb drive and electrical isolation trenches are annotated. With an application of a bias voltage across the comb drive, an electrostatic attractive force is generated that changes the coupling gap between the waveguides. This change in gap width varies the power split between the waveguides. (b) Plot showing the measured optical power from both drop and through ports for different applied actuation voltages.

3.3 Hermetic Sealing

The optical waveguides inside the MEMS cavities are free-standing, making them susceptible to environmental influences. A wafer-level hermetic sealing process was developed to protect the MEMS from environmental influences.[67,68] Therefore, a thermo-compression bonding process was used to create a metal-to-metal bond between a Au/TiW layer on the sealing lid and the aluminum copper sealing rims on the silicon photonic device wafer. As the bonding process is carried out in a vacuum chamber, a vacuum atmosphere is established inside the hermetically sealed cavities.[69] Figure 6 shows pictures of the un-diced sealed wafer and a sealed chip after dicing. The sealing yield of the MEMS cavities was found to be bttere than 96% even after two months of storing the sealed MEMS cavities. The high sealing yield was observed even after the dicing of the wafer into separate chips.

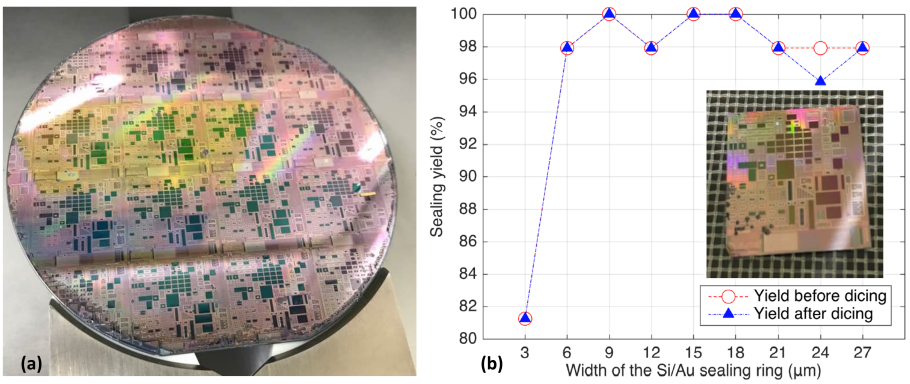


Figure 6. (a) Picture of an un-diced post-processed and sealed wafer. (b) Plot showing the measured sealing yield before and after the dicing of the wafer with the hermetically sealed cavities. The inset shows a picture of an individual chip that has been diced from the sealed and processed wafer.

Downloaded From: https://www.spiedigitallibrary.org/conference-proceedings-of-spie on 24 Mar 2023
Terms of Use: https://www.spiedigitallibrary.org/terms-of-use

4. LIQUID CRYSTALS (LC)

Birefringence of materials like liquid crystals (LC) consisting of anisotropic rod-like molecules (having a short and a long axis) can be used to manipulate light on a chip. The birefringence is characterized by the director which is a vector aligned along the long axis of the anisotropic molecules. Earlier experiments with LC around optical waveguides show that the director tends to align itself along the propagation direction of the waveguides in the equilibrium state (i.e. when no voltage is applied) due to the molecular surface interactions.[70,71] When a voltage above a certain threshold is applied over the LC, the director tries to align itself with the electric field. This alignment with the electric field depends on the strength of the applied voltage as the electric field competes with the elasticity of the material pulling it back to its equilibrium state. This means that LC director orientation can be controlled by varying the strength of an electric field (the voltage) leading to a change in the refractive index around the waveguide. This mechanism allows tuning of the effective index of an optical waveguide mode. Early experiments using LC-actuation required high voltages[71] for actuation because the electrodes were positioned at a large distance from the waveguides to avoid absorption. Low-voltage liquid crystal phase shifts have also been demonstrated using slot waveguides but this technique suffered from high insertion losses due to the transitions and propagation in a narrow slot.[24] As discussed above, programmable photonic circuits require low-power actuators along with high-speed library components from a standard silicon photonics platform. So, we have developed a process flow to enhance the established silicon photonic platform from IMEC, iSiPP50G, with LC-based phase shifters.

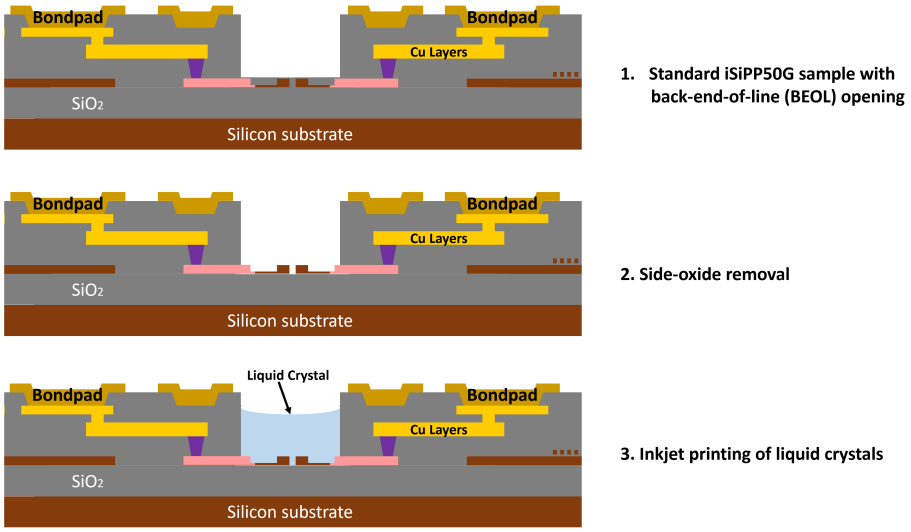


Figure 7. Sketches showing the cross-sections of the device area after major steps of the process flow. Step 1 represents the state after the removal of *back-end-of-line* (BEOL) stack using the standard iSiPP50G module. Step 2 represents the state after the removal of the side oxide cladding using *buffered hydrofluoric acid* (bHF). Step 3 represents the state after the inkjet printing of liquid crystal molecules into the recess. It should be mentioned here that the first two steps are exactly the same as those of the MEMS post-processing flow.

Figure 7 summarizes the developed process flow for the enhancement of the iSiPP50G silicon photonics platform with LC-based actuators. The first two steps of the process flow are the same as that of the process flow developed for MEMS enhancement of the platform (see Figure 3). After the removal of the side oxide in step 2, recess is filled with liquid crystal (we use a commercially available mixture called E7) with inkjet printing.[72] Inkjet printing was used as it enables localized and controlled deposition within the recess without any spillage. A schematic cross-section of the sample after inkjet printing of liquid crystal is shown in step 3 of Figure 7.

The designed LC-based phase shifter shown in Figure 8 (a) consists of an optical waveguide and an intrinsic (undoped) silicon electrode residing in close proximity of the waveguide (note the similarity between the silicon electrode and the movable narrow silicon beam in the MEMS phase shifter devices explained earlier).[31] It can be noticed in Figure 8 (a) that the silicon electrode is connected to the metal contact outside the recess. Doped

Downloaded From: https://www.spiedigitallibrary.org/conference-proceedings-of-spie on 24 Mar 2023
Terms of Use: https://www.spiedigitallibrary.org/terms-of-use

silicon is used as much as possible to lower the resistivity of electrical connections to the intrinsic silicon electrode. The silicon electrode has a small width, which puts it in optical cut-off at the operation wavelength of 1550 nm and thus inhibits any optical coupling. Due to the close proximity of the electrode, high field strengths are possible within the gap between the waveguide (which serves as the electrical ground) and the electrode at low voltages. This layout has a higher $V_\pi L_\pi$ compared to slot waveguide infiltrated phase shifters with very low $V_\pi L_\pi$,[24] but exhibits a lower insertion loss because the transitions (tapers) between the regular waveguide and slot waveguide are avoided.

As described earlier, the director aligns itself along the propagation direction of the waveguide in the equilibrium state (i.e. when no voltage is applied). When a voltage is applied over the gap between the electrode and the grounded waveguide, the director re-orients itself towards the electric field within the gap between the waveguide and the silicon electrode. The amount of re-orientation depends on the applied voltage and results in a change of the refractive index in the cladding of the single-mode waveguide, which induces a phase shift. It should be mentioned here that the polarity of the applied voltage needs to reverse frequently at a particular rate (square wave as an electronic signal) to avoid ion drift.[31]

To characterize the phase shift induced by the LC-based phase shifter, an unbalanced *Mach-Zehnder interferometer* (MZI) was designed having a LC phase shifter in one of the paths. After inkjet printing of the commercially available liquid crystal mixture E7, a square wave of 20 kHz was applied to the bond-pad connected to the silicon electrode for voltages up to 9 Vrms. Measured transmission responses for different values of applied voltages are shown in Figure 8 (c). The noise on the measured transmission responses is due to the phase flicker.[23,31] Extracted phase shifts for varying gaps between the waveguide and the electrode are plotted in Figure 8 (d). It can be noticed that a phase shift of almost 3π was achieved for a voltage of 9 Vrms for a gap of 200 nm.

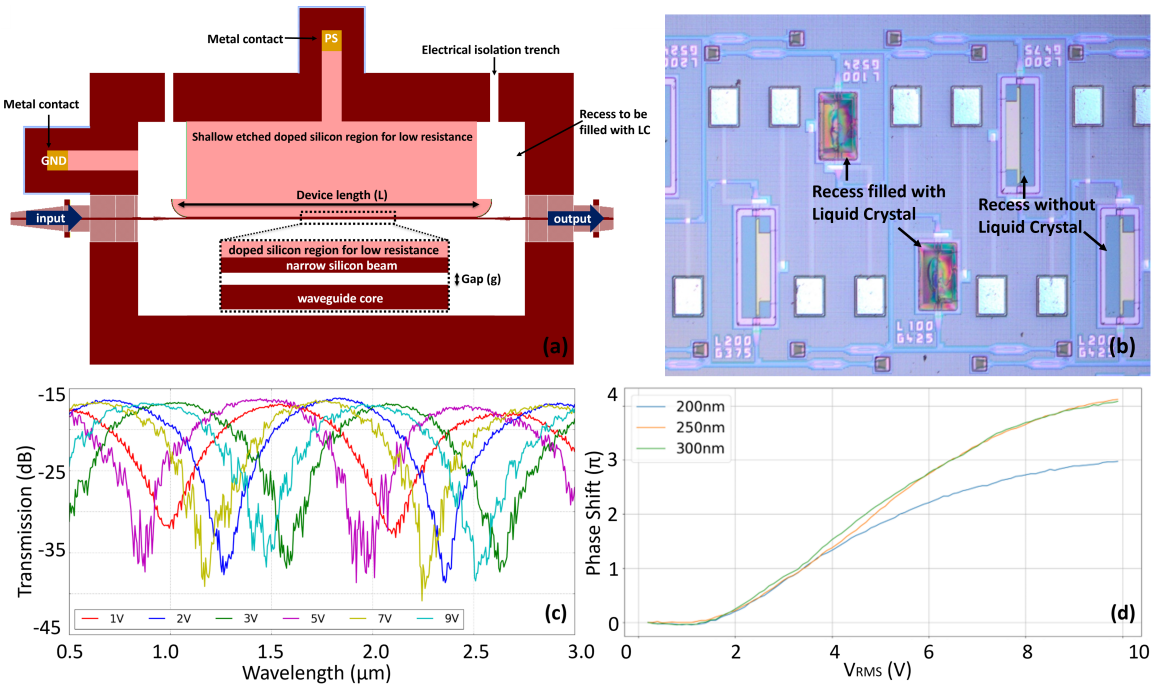


Figure 8. (a) Sketch showing the LC based phase shifter. Optical waveguide and the neighbouring narrow silicon electrode can be observed in the inset showing the zoomed in image. Metal connections, the gap between the waveguide and the narrow silicon electrode, device length, doped silicon regions and optical ports are annotated. (b) Microscope image of a fabricated silicon photonic chip. Recesses filled with liquid crystal using inkjet printing are annotated. (c) Plots showing the transmission responses measured for different values of applied voltages. (d) Plots showing experimentally extracted phase shift values corresponding to different applied voltages.

Downloaded From: https://www.spiedigitallibrary.org/conference-proceedings-of-spie on 24 Mar 2023
Terms of Use: https://www.spiedigitallibrary.org/terms-of-use

5. SUMMARY

This paper presents the latest developments in enhancing an established silicon photonics platform from IMEC (iSiPP50G) with low-power *micro-electromechanical system* (MEMS) and *liquid crystal* (LC) actuators to enable general-purpose large-scale programmable *photonic integrated circuits* (PICs).

ACKNOWLEDGMENTS

The results in this work are supported by the European Union through the H2020 project MORPHIC (grant 780283), Horizon Europe project PHORMIC (grant 101070332) and the ERC grant PhotonicSWARM (grant 725555).

REFERENCES

[1] Soref, R., "The past, present, and future of silicon photonics," *IEEE Journal of selected topics in quantum electronics* **12**(6), 1678–1687 (2006).

[2] Koch, T. L. and Koren, U., "Semiconductor photonic integrated circuits," *IEEE Journal of Quantum Electronics* **27**(3), 641–653 (1991).

[3] Duan, X., Huang, Y., Cui, Y., Wang, J., and Lieber, C. M., "Indium phosphide nanowires as building blocks for nanoscale electronic and optoelectronic devices," *Nature* **409**(6816), 66 (2001).

[4] Khan, M. U., Xing, Y., Ye, Y., and Bogaerts, W., "Photonic integrated circuit design in a foundry+fabless ecosystem," *IEEE J. Sel. Top. Quant. Electron.* **25**(5), 1–14 (2019).

[5] Sharma, T., Wang, J., Kaushik, B. K., Cheng, Z., Kumar, R., Wei, Z., and Li, X., "Review of recent progress on silicon nitride-based photonic integrated circuits," *IEEE Access* **8**, 195436–195446 (2020).

[6] Khan, M. U., Justice, J., Petäjä, J., Korhonen, T., Boersma, A., Wiegersma, S., Karppinen, M., and Corbett, B., "Multi-level single mode 2d polymer waveguide optical interconnects using nano-imprint lithography," *Optics Express* **23**(11), 14630–14639 (2015).

[7] Wörhoff, K., Heideman, R. G., Leinse, A., and Hoekman, M., "Triplex: a versatile dielectric photonic platform," *Advanced Optical Technologies* **4**(2), 189–207 (2015).

[8] Khan, M. U., McGrath, J., Corbett, B., and Pemble, M., "Air-clad broadband waveguide using micro-molded polyimide combined with a robust, silica-based inverted opal substrate," *Optical Materials Express* **7**(9), 3155–3161 (2017).

[9] Xing, Y., Dong, J., Khan, U., and Bogaerts, W., "Capturing the effects of spatial process variations in silicon photonic circuits," *ACS Photonics* (2022).

[10] Chrostowski, L., Wang, X., Flueckiger, J., Wu, Y., Wang, Y., and Fard, S. T., "Impact of fabrication non-uniformity on chip-scale silicon photonic integrated circuits," in [*Conference on Optical Fiber Communication, Technical Digest Series*], Th2A–37, Optical Society of America (2014).

[11] Bogaerts, W., Khan, U., and Xing, Y., "Layout-aware yield prediction of photonic circuits," in [*2018 IEEE 15th International Conference on Group IV Photonics (GFP)*], 1–2, Ieee (2018).

[12] Bogaerts, W., Pérez, D., Capmany, J., Miller, D. A., Poon, J., Englund, D., Morichetti, F., and Melloni, A., "Programmable photonic circuits," *Nature* **586**(7828), 207–216 (2020).

[13] Harris, N. C., Carolan, J., Bunandar, D., Prabhu, M., Hochberg, M., Baehr-Jones, T., Fanto, M. L., Smith, A. M., Tison, C. C., Alsing, P. M., and Englund, D., "Linear programmable nanophotonic processors," *Optica* **5**(12), 1623–1631 (2018).

[14] Pérez, D., Gasulla, I., and Capmany, J., "Field-programmable photonic arrays," *Optics Express* **26**(21), 27265 (2018).

[15] Bogaerts, W., Edinger, P., Takabayashi, A. Y., Zand, I., Chen, X., Wang, X., Sattari, H., Verheyen, P., Jezzini, M. A., Talli, G., et al., "Building large-scale programmable photonic circuits using silicon photonic mems," in [*Photonics in Switching and Computing*], PsTh1F–1, Optical Society of America (2020).

[16] Khan, U., Zand, I., Edinger, P., Jo, G., Bleiker, S. J., Takabayashi, A. Y., Antony, C., Lee, J., Malik, A. K., Verheyen, P., et al., "Large scale programmable photonic circuits using silicon photonic mems," in [*2022 Conference on Lasers and Electro-Optics (CLEO)*], 1–2, IEEE (2022).

Downloaded From: https://www.spiedigitallibrary.org/conference-proceedings-of-spie on 24 Mar 2023
Terms of Use: https://www.spiedigitallibrary.org/terms-of-use

[17] Khan, U., Zand, I., Edinger, P., Jo, G., Bleiker, S. J., Takabayashi, A. Y., Antony, C., Jezzini, M., Talli, G., Sattari, H., et al., "Morphic: Mems enhanced silicon photonics for programmable photonics," in [*Integrated Photonics Platforms II*], **12148**, 97–106, SPIE (2022).

[18] Masood, A., Pantouvaki, M., Goossens, D., Lepage, G., Verheyen, P., Van Thourhout, D., Absil, P., and Bogaerts, W., "CMOS-compatible Tungsten heaters for silicon photonic waveguides," in [*IEEE International Conference on Group IV Photonics GFP*], 234–236 (2012).

[19] Gan, F., Barwicz, T., Popovic, M., Dahlem, M., Holzwarth, C., Rakich, P., Smith, H., Ippen, E., and Kartner, F., "Maximizing the thermo-optic tuning range of silicon photonic structures," in [*2007 Photonics in Switching*], 67–68, IEEE (2007).

[20] Fang, Q., Song, J. F., Liow, T.-Y., Cai, H., Yu, M. B., Lo, G. Q., and Kwong, D.-L., "Ultralow power silicon photonics thermo-optic switch with suspended phase arms," *IEEE Photonics Technology Letters* **23**(8), 525–527 (2011).

[21] Witzens, J., "High-Speed Silicon Photonics Modulators," *Proceedings of the IEEE* **106**, 2158–2182 (12 2018).

[22] Reed, G. T., Mashanovich, G., Gardes, F. Y., and Thomson, D. J., "Silicon optical modulators," *Nature Photonics* **4**(8), 518–526 (2010).

[23] Van Iseghem, L., Khan, U., Edinger, P., Errando-Herranz, C., Takabayashi, A. Y., Sattari, H., Gylfason, K. B., Quack, N., Beeckman, J., and Bogaerts, W., "Liquid crystal phase shifter integrated in a silicon photonics platform," in [*22nd European Conference on Integrated Optics, ECIO 2020*], (2020).

[24] Xing, Y., Ako, T., George, J. P., Korn, D., Yu, H., Verheyen, P., Pantouvaki, M., Lepage, G., Absil, P., Ruocco, A., et al., "Digitally controlled phase shifter using an soi slot waveguide with liquid crystal infiltration," *IEEE Photonics Technology Letters* **27**(12), 1269–1272 (2015).

[25] Wei, T., Chen, P., Tang, M.-J., Wu, G.-X., Chen, Z.-X., Shen, Z.-X., Ge, S.-J., Xu, F., Hu, W., and Lu, Y.-Q., "Liquid-crystal-mediated active waveguides toward programmable integrated optics," *Advanced Optical Materials* **8**(10), 1902033 (2020).

[26] Berteloot, B., Nys, I., Xue, X., Beeckman, J., and Neyts, K., "Rotationally invariant ring-shaped liquid crystal structures between two substrates with different photoalignment," *Journal of Molecular Liquids* **337**, 116238 (2021).

[27] De Cort, W., Beeckman, J., Claes, T., Neyts, K., and Baets, R., "Wide tuning of silicon-on-insulator ring resonators with a liquid crystal cladding," *Opt. Lett.* **36**, 3876–3878 (Oct. 2011).

[28] Wang, C.-T., Li, Y.-C., Yu, J.-H., Wang, C. Y., Tseng, C.-W., Jau, H.-C., Chen, Y.-J., and Lin, T.-H., "Electrically tunable high q-factor micro-ring resonator based on blue phase liquid crystal cladding," *Optics Express* **22**, 17776–17781 (JUL 28 2014).

[29] Ako, T., Hope, A., Nguyen, T., Mitchell, A., Bogaerts, W., Neyts, K., and Beeckman, J., "Electrically tuneable lateral leakage loss in liquid crystal clad shallow-etched silicon waveguides," *OPTICS EXPRESS* **23**, 2846–2856 (FEB 9 2015).

[30] Atsumi, Y., Watabe, K., Uda, N., Miura, N., and Sakakibara, Y., "Initial alignment control technique using on-chip groove arrays for liquid crystal hybrid silicon optical phase shifters," *OPTICS EXPRESS* **27**, 8756–8767 (MAR 18 2019).

[31] Van Iseghem, L., Picavet, E., Takabayashi, A. Y., Edinger, P., Khan, U., Verheyen, P., Quack, N., Gylfason, K. B., De Buysser, K., Beeckman, J., et al., "Low power optical phase shifter using liquid crystal actuation on a silicon photonics platform," *Optical Materials Express* **12**(6), 2181–2198 (2022).

[32] Abel, S., Eltes, F., Ortmann, J. E., Messner, A., Castera, P., Wagner, T., Urbonas, D., Rosa, A., Gutierrez, A. M., Tulli, D., Ma, P., Baeuerle, B., Josten, A., Heni, W., Caimi, D., Czornomaz, L., Demkov, A. A., Leuthold, J., Sanchis, P., and Fompeyrine, J., "Large Pockels effect in micro- and nanostructured barium titanate integrated on silicon," *Nature Materials* **18**(1), 42–47 (2019).

[33] Leuthold, J., Koos, C., Freude, W., Alloatti, L., Palmer, R., Korn, D., Pfeifle, J., Lauermann, M., Dinu, R., Wehrli, S., Jazbinsek, M., Günter, P., Waldow, M., Wahlbrink, T., Bolten, J., Kurz, H., Fournier, M., Fedeli, J.-M. J. M., Yu, H., Bogaerts, W., Gunter, P., Waldow, M., Wahlbrink, T., Bolten, J., Kurz, H., Fournier, M., Fedeli, J.-M. J. M., Yu, H., and Bogaerts, W., "Silicon-Organic hybrid electro-optical devices," *IEEE Journal on Selected Topics in Quantum Electronics* **19**, 114–126 (11 2013).

Downloaded From: https://www.spiedigitallibrary.org/conference-proceedings-of-spie on 24 Mar 2023
Terms of Use: https://www.spiedigitallibrary.org/terms-of-use

[34] Sun, H., Qiao, Q., Guan, Q., and Zhou, G., "Silicon photonic phase shifters and their applications: A review," *Micromachines* **13**(9), 1509 (2022).

[35] Parra, J., Hurtado, J., Griol, A., and Sanchis, P., "Ultra-low loss hybrid ito/si thermo-optic phase shifter with optimized power consumption," *Optics Express* **28**(7), 9393–9404 (2020).

[36] Sun, P. and Reano, R. M., "Submilliwatt thermo-optic switches using free-standing silicon-on-insulator strip waveguides," *Optics express* **18**(8), 8406–8411 (2010).

[37] Liu, M., Yin, X., and Zhang, X., "Double-layer graphene optical modulator," *Nano letters* **12**(3), 1482–1485 (2012).

[38] Chiles, J. and Fathpour, S., "Mid-infrared integrated waveguide modulators based on silicon-on-lithium-niobate photonics," *Optica* **1**(5), 350–355 (2014).

[39] Van Acoleyen, K., Roels, J., Mechet, P., Claes, T., Van Thourhout, D., and Baets, R., "Ultracompact phase modulator based on a cascade of NEMS-operated slot waveguides fabricated in silicon-on-insulator," *IEEE Photonics Journal* **4**, 779–788 (6 2012).

[40] Liu, T., Pagliano, F., Van Veldhoven, R., Pogoretskii, V., Jiao, Y., and Fiore, A., "InP MEMS Mach-Zehnder interferometer optical switch on silicon," *European Conference on Integrated Optics (ECIO)* (2019).

[41] Edinger, P., Takabayashi, A. Y., Errando-Herranz, C., Khan, U., Sattari, H., Verheyen, P., Bogaerts, W., Quack, N., and Gylfason, K. B., "Silicon photonic microelectromechanical phase shifters for scalable programmable photonics," *Optics Letters* **46**, 5671 (11 2021).

[42] Baghdadi, R., Gould, M., Gupta, S., Tymchenko, M., Bunandar, D., Ramey, C., and Harris, N. C., "Dual slot-mode NOEM phase shifter," *Optics Express* **29**, 19113 (6 2021).

[43] Grottke, T., Hartmann, W., Schuck, C., and Pernice, W. H. P., "Optoelectromechanical phase shifter with low insertion loss and a 13π tuning range," *Optics Express* **29**, 5525 (2 2021).

[44] Abe, S. and Hane, K., "Variable-gap silicon photonic waveguide coupler switch with a nanolatch mechanism," *IEEE Photonics Technology Letters* **25**(7), 675–677 (2013).

[45] Sattari, H., Takabayashi, A. Y., Zhang, Y., Verheyen, P., Bogaerts, W., and Quack, N., "Compact broadband suspended silicon photonic directional coupler," *Optics Letters* **45**, 2997 (6 2020).

[46] Seok, T. J., Quack, N., Han, S., Muller, R. S., and Wu, M. C., "Highly Scalable Digital Silicon Photonic MEMS Switches," *Journal of Lightwave Technology* **34**, 365–371 (1 2016).

[47] Seok, T. J., Kwon, K., Henriksson, J., Luo, J., and Wu, M. C., "Wafer-scale silicon photonic switches beyond die size limit," *Optica* **6**, 490 (4 2019).

[48] Bulgan, E., Kanamori, Y., and Hane, K., "Submicron silicon waveguide optical switch driven by microelectromechanical actuator," *Applied Physics Letters* **92**(10), 1–4 (2008).

[49] Takabayashi, A. Y., Sattari, H., Edinger, P., Verheyen, P., Gylfason, K. B., Bogaerts, W., and Quack, N., "Broadband Compact Single-Pole Double-Throw Silicon Photonic MEMS Switch," *Journal of Microelectromechanical Systems* **30**, 322–329 (4 2021).

[50] Edinger, P., Takabayashi, A. Y., Errando-Herranz, C., Khan, U., Antony, C., Talli, G., Verheyen, P., Bogaerts, W., Quack, N., and Gylfason, K. B., "A bistable silicon photonic mems phase switch for nonvolatile photonic circuits," in [*2022 IEEE 35th International Conference on Micro Electro Mechanical Systems Conference (MEMS)*], 995–997, IEEE (2022).

[51] Chu, H. M. and Hane, K., "A wide-tuning silicon ring-resonator composed of coupled freestanding waveguides," *IEEE Photonics Technology Letters* **26**(14), 1411–1413 (2014).

[52] Edinger, P., Van Nguyen, C. P., Takabayashi, A. Y., Antony, C., Talli, G., Verheyen, P., Khan, U., Bogaerts, W., Quack, N., and Gylfason, K. B., "Add-drop silicon ring resonator with low-power mems tuning of phase and coupling," in [*2022 Conference on Lasers and Electro-Optics (CLEO)*], 1–2, IEEE (2022).

[53] Pantouvaki, M., Srinivasan, S. A., Ban, Y., De Heyn, P., Verheyen, P., Lepage, G., Chen, H., De Coster, J., Golshani, N., Balakrishnan, S., Absil, P., Van Campenhout, J., Coster, J. D., Campenhout, J. V., Pantouvaki, M., Golshani, N., Absil, P., Heyn, P. D., Verheyen, P., Balakrishnan, S., Srinivasan, S. A., Ban, Y., De Heyn, P., Verheyen, P., Lepage, G., Chen, H., De Coster, J., Golshani, N., Balakrishnan, S., Absil, P., and Van Campenhout, J., "Active Components for 50 Gb/s NRZ-OOK Optical Interconnects in a Silicon Photonics Platform," *Journal of Lightwave Technology* **35**, 631–638 (2 2017).

Downloaded From: https://www.spiedigitallibrary.org/conference-proceedings-of-spie on 24 Mar 2023
Terms of Use: https://www.spiedigitallibrary.org/terms-of-use

[54] Bogaerts, W., Yuji Takabayashi, A., Edinger, P., Jo, G., Zand, I., Verheyen, P., Jezzini, M., Sattari, H., Talli, G., Antony, C., Saei, M., Lerma Arce, C., Su Lee, J., Kumar Mallik, A., Kumar, S., Garcia, M., Jonuzi, T., B. Gylfason, K., Quack, N., Niklaus, F., and Khan, U., "Programmable silicon photonic circuits powered by mems," *Proc. SPIE* **12005**, 1200509 (2022).

[55] Quack, N., Sattari, H., Takabayashi, A. Y., Zhang, Y., Verheyen, P., Bogaerts, W., Edinger, P., Errando-Herranz, C., and Gylfason, K. B., "Mems-enabled silicon photonic integrated devices and circuits," *IEEE Journal of Quantum Electronics* **56**(1), 1–10 (2019).

[56] Agrawal, G. P., "Nonlinear fiber optics: its history and recent progress," *JOSA B* **28**(12), A1–A10 (2011).

[57] Lu, Z., Yun, H., Wang, Y., Chen, Z., Zhang, F., Jaeger, N. A. F., and Chrostowski, L., "Broadband silicon photonic directional coupler using asymmetric-waveguide based phase control," *Optics Express* **23**, 3795 (2 2015).

[58] Yariv, A., "Coupled-mode theory for guided-wave optics," *IEEE Journal of Quantum Electronics* **9**(9), 919–933 (1973).

[59] Xing, Y., Khan, U., Alves Júnior, A. R., and Bogaerts, W., "Behavior model for directional coupler," in [*Proceedings Symposium IEEE Photonics Society Benelux*], 128–131 (2017).

[60] Soldano, L. B. and Pennings, E. C., "Optical multi-mode interference devices based on self-imaging: principles and applications," *Journal of lightwave technology* **13**(4), 615–627 (1995).

[61] Le, T. T. and Cahill, L. W., "The design of multimode interference couplers with arbitrary power splitting ratios on an soi platform," in [*LEOS 2008-21st Annual Meeting of the IEEE Lasers and Electro-Optics Society*], 378–379, IEEE (2008).

[62] Chiang, K. S. and Liu, Q., "Formulae for the design of polarization-insensitive multimode interference couplers," *IEEE Photonics Technology Letters* **23**(18), 1277–1279 (2011).

[63] Besse, P. A., Bachmann, M., Melchior, H., Soldano, L. B., and Smit, M. K., "Optical bandwidth and fabrication tolerances of multimode interference couplers," *Journal of Lightwave Technology* **12**(6), 1004–1009 (1994).

[64] Wang, M., Chen, X., Khan, U., and Bogaerts, W., "Programmable wavelength filter with double ring loaded mzi," *Scientific Reports* **12**(1), 1–12 (2022).

[65] Miller, D. A., "Perfect optics with imperfect components," *Optica* **2**(8), 747–750 (2015).

[66] Suzuki, K., Cong, G., Tanizawa, K., Kim, S.-H., Ikeda, K., Namiki, S., and Kawashima, H., "Ultra-high-extinction-ratio 2× 2 silicon optical switch with variable splitter," *Optics express* **23**(7), 9086–9092 (2015).

[67] Wang, X., Bleiker, S. J., Edinger, P., Errando-Herranz, C., Roxhed, N., Stemme, G., Gylfason, K. B., and Niklaus, F., "Wafer-level vacuum sealing by transfer bonding of silicon caps for small footprint and ultra-thin MEMS packages," *Journal of Microelectromechanical Systems* **28**(3), 460–471 (2019).

[68] Jo, G., Edinger, P., Bleiker, S., Wang, X., Takabayashi, A. Y., Sattari, H., Quack, N., Jezzini de Anda, M. A., Verheyen, P., Stemme, G., Bogaerts, W., Gylfason, K. B., and Niklaus, F., "Wafer-level vacuum sealing for packaging of silicon photonic MEMS," in [*Silicon Photonics XVI*], Reed, G. T. and Knights, A. P., eds., 11, SPIE (3 2021).

[69] Jo, G., Edinger, P., Bleiker, S., Wang, X., Takabayashi, A., Sattari, H., Quack, N., Jezzini, M., Verheyen, P., Zand, I., Khan, U., Bogaerts, W., Stemme, G., Gylfason, K., and Niklaus, F., "Wafer-level Hermetically Sealed Silicon Photonic MEMS," *Photonics Research* **10**, 14 (11 2021).

[70] De Cort, W., Beeckman, J., James, R., Fernandez, F. A., Baets, R., and Neyts, K., "Tuning silicon-on-insulator ring resonators with in-plane switching liquid crystals," *JOSA B* **28**(1), 79–85 (2011).

[71] De Cort, W., Beeckman, J., Claes, T., Neyts, K., and Baets, R., "Wide tuning of silicon-on-insulator ring resonators with a liquid crystal cladding," *Optics letters* **36**(19), 3876–3878 (2011).

[72] Moirangthem, M., Scheers, A. F., and Schenning, A. P., "A full color photonic polymer, rewritable with a liquid crystal ink," *Chemical Communications* **54**(35), 4425–4428 (2018).

Downloaded From: https://www.spiedigitallibrary.org/conference-proceedings-of-spie on 24 Mar 2023
Terms of Use: https://www.spiedigitallibrary.org/terms-of-use